1 **Investigation of the functional relationship between antecedent rainfall and the probability**

2 **of debris flow occurrence in Jiangjia Gully, China**

3 Shaojie Zhang[1], Xiaohu Lei[1,4], Hongjuan Yang[1], Kaiheng Hu[1], Juan Ma[2], Dunlong Liu[3], Fanqiang Wei[4]

4 1.State Key Laboratory of Mountain Hazards and Engineering Safety, Institute of Mountain Hazards and

5 Environment, Chinese Academy of Sciences, Chengdu 610041, China

6 2.China Institute for Geo-Environment Monitoring, Beijing, 100081

7 3.College of Software Engineering, Chengdu University of Information and Technology, Chengdu, 610225, China

8 4.Chongqing Institute of Green and Intelligent Technology, Chinese Academy of Sciences, Chongqing 400714,

9 China

10 Correspondence to: Shaojie Zhang, E-mail: sj-zhang@imde.ac.cn; Kaiheng Hu, E-mail: khhu@imde.ac.cn

11 **Abstract**

12 A larger antecedent effective precipitation (AEP) indicates a higher probability of a debris flow

13 (P_{df}) being triggered by subsequent rainfall. Scientific topics surrounding this qualitative conclusion

14 that can be raised, including what kinds of variation rules do they follow, and whether there is a

15 boundary limit. To answer these questions, Jiangjia Gully in Dongchuan, Yunnan province, China,

16 is chosen as the study area, and a numerical calculation, rainfall scenario simulation, and Monte

17 Carlo integration method have been used to calculate the occurrence probability of debris flow under

18 different AEP conditions and derive the functional relationship between P_{df} and AEP. The

19 relationship between P_{df} and AEP can be quantified by a piecewise function. P_{df} is equal to 15.88%

20 even AEP reaches 85 mm indicating that debris flow in nature has an extremely small probability

21 compared to the rainfall frequency. Data from 1094 rainfall events and 37 historical debris flow

22   events are collected to verify the reasonability of the functional relationship. The results indicate

23   that the piecewise function are highly correlated with the observation results. Our study confirms

24   the correctness of the qualitative description of the relationship between AEP and P_{df}, clarifies that

25   debris flow is a small probability event compared to rainfall frequency, and quantitatively reveals

26   the evolution law of debris flow occurrence probability with AEP, which can provide a clear

27   reference for the early warning of debris flows.

28   **Keywords:** Debris flow, antecedent effective rainfall, Dens-ID, Monte Carlo method

30   **1 Introductions**

31   The antecedent effective precipitation (AEP) likes a Trojan horse lurking inside a loose soil

32   mass, which can cooperate with subsequent rainfall at any time to trigger debris flow in a debris-

33   flow gully. The AEP is equivalent to the precipitation preserved in soil mass before the triggering

34   rainfall process; it represents the saturation degree of loose soil mass (Segoni et al., 2018a;

35   Leonarduzz and Molnar, 2020). Therefore, the soil moisture that has accumulated from antecedent

36   rainfall since the beginning of a rainfall season has a significant influence on how new storm rainfall

37   interacts with the loose soil mass within a gully (Fiorillo and Wilson, 2004; Long et al., 2020). The

38   increase in AEP can decrease the shear strength of a loose solid material provided by shallow

39   landslides or channel erosion (Papa, et al., 2013; Senthilkumar et al., 2017; Liu et al., 2020), as a

40   consequence, the supply rate of solid material resources can be significantly enhanced in the

41   subsequent rainfall process (Wei et al., 2008; Bennett et al., 2014; Zhang et al., 2020). Additionally,

42   increased AEP and moisture content have been shown to enhance rainfall-induced surface runoff in

43   a variety of environments (Tisdall, 1951; Luk, 1985; Le Bissonnais et al., 1995; Castillo et al., 2003;

44   Jones et al., 2017; Hirschberg et al., 2021). Thus, AEP plays an important role in the formation of

45   debris flows (Hong et al., 2018).

46   Rainfall thresholds represent the difficulty degree of debris flow triggered by rainfall (Marra

47   et al., 2017). Investigations including the influence of AEP on the rainfall threshold can be helpful

48   to examining the relationship between AEP and debris flow occurrence. Currently, the relationship

49   between the AEP and rainfall threshold indicates that there is a negative correlation between the

50   AEP and rainfall conditions that trigger debris flows (Huang, 2013). AEP also represents the

51   saturation degree of loose soil mass (Zhao et al., 2019a; Abraham et al., 2021), and integrating soil

52   moisture with rainfall thresholds has been proven effective in improving prediction performance

53   (Segoni et al., 2018a; Zhao et al., 2019b; Abraham et al., 2020). Scholars also have attempted to

54   analyze the influence of antecedent soil moisture on the rainfall threshold triggering debris flow

55   (Cui et al., 2007; Hu et al., 2015), and there is still a negative correlation between antecedent soil

56   moisture and triggering rainfall conditions (Chen et al., 2017) just like the relationship between AEP

57   and rainfall threshold. The above investigations show that increasing in AEP can significantly

58   decrease the rainfall conditions for triggering a debris flow, which in turn means that debris flow is

59   more likely to occur. Generally, the qualitative description of 'the greater the AEP, the higher the

60   probability (P_{df}) of subsequent rainfall triggering the debris flow (De Vita et al., 2000; Bel et al.,

61   2017)' has gradually become a consensus. Therefore, discovering a specific function to describe this

62   qualitative description is helpful to further demonstrating the above consensus, revealing a certain

63   evolutionary law of debris flow with rainfall in nature.

64   To quantify the evolution law of P_{df} with the changing AEP, a numerical model denoted as the

65   Dens-ID can correlate the rainfall parameters (I and D) with the debris flow density (Zhang et al.,

2020; Long et al., 2020; Zhang et al., 2023), and it has been used to construct the rainfall intensity-duration (ID) threshold curves under different AEP conditions. The ID threshold curves with upper and lower bounds can delineate the closed region in the ID coordinate system, which represents the set of all rainfall conditions that can trigger debris flow at a certain AEP. Consequently, the probability of natural rainfall falling into a closed region is equivalent to P_{df}, which can then be calculated based on Monte Carlo integration. The next section introduces the basic information of study area including the rainfall and debris flow event data collected from the study area. The third section addresses how to establish the functional relationship between the AEP and Pdf using the Dens-ID and Monte Carlo integration method. Section 4, 5 and 6 discuss the results and state the conclusions of this study, respectively.

2 Study areas

The Jiangjia Gully (JJG) is a primary tributary of the Xiaojiang River, which is located in the Dongchuan District of Kunming City, Yunnan Province, China (Fig.1). As shown in Fig.1, JJG has a drainage area of 48.6 km^2 with elevations ranging from 1040to 3260 m. In this gully, the relative relief from the ridge to the valley reaches 500 m, and most of the slope gradient is greater than 25°. Slopes within JJG are covered by abundant loose soil with a thickness of more than ten meters. Shallow landslides are frequently triggered by intense rainfall processes in JJG, providing a large number of solid materials for debris flow (Yang et al., 2022). Before 1979, the Menqian and Duozhao gullies are the two main tributaries of JJG, accounting for 64.7% of the entire drainage area. The upstream areas of the two main tributaries are the initiation zones of the debris flows, and the channels of the upstream tributaries are narrow and V-shaped (Zhang et al., 2020). However, several check dams have been constructed in the Duozhao gully since 1979, which have significantly reduced debris flow activity in this sub-gully (Zeng et al., 2009). Currently, Menqian Gully with the area of 13.2 km^2 is the primary source area. The slope gradient of its both sides is very steep, e.g., the mean slope in Menqian Gully is 32° and the maximum slope can reach 70°.

Bedrock that mainly consists of slates formed in lower Proterozoic crops out in the unvegetated or sparsely vegetated lower part. The bedrock is fragmented and mostly disintegrates into clasts with the size more than 20 mm. The upper part of the bedrock is lain by soil mantles with thicknesses of 0.5–20 m, which are covered by grasses and shrubs, or are used for terrace farming. The soil mantle is poorly sorted and composed of particles from clay to boulder. The translational zone from the upper to the lower parts of the slope is prone to shallow landslides. Some landslides directly evolve into debris flows, while the others release sediment to the channel, which is mobilized by runoff in debris flow events (Yang et al., 2022).
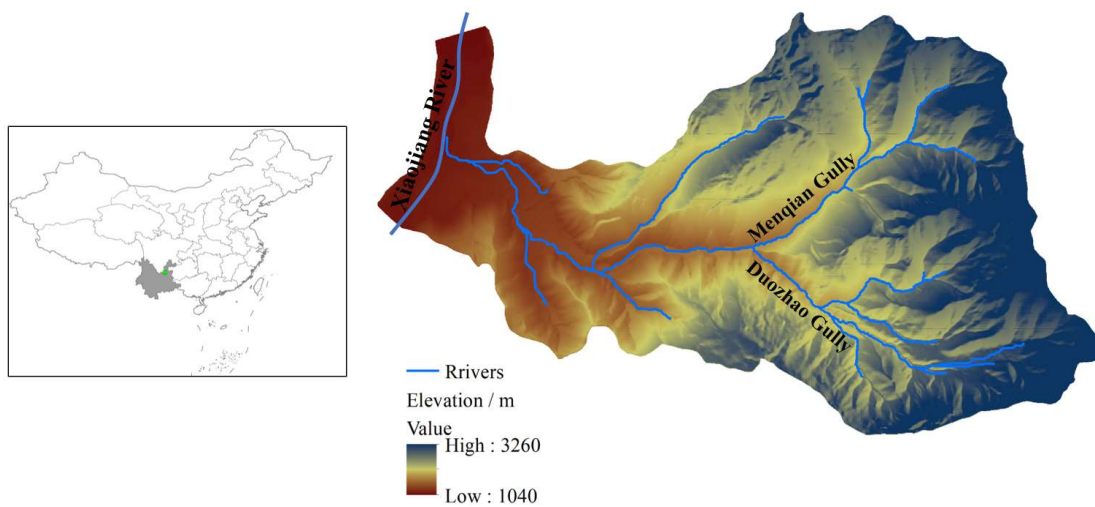
Fig.1 Location of JJG

Steep terrain provides a beneficial potential energy condition for transporting a large amount of loose solid materials from JJG to Xiaojiang River. Consequently, debris flows in JJG can be easily triggered by high-intensity rainstorm or long-duration rainfall processes (Zhang et al., 2020). The solid material necessary for a debris flow in a gully may be from shallow landslides (Iverson et al., 1997; Gabet and Mudd, 2006; Zhang et al., 2020; Long et al., 2020) or runoff-induced bed erosions (Berti and Simoni, 2005; Coe et al., 2008; Tang et al., 2020; Bernard and Gregoretti, 2021). In JJG, shallow landslides are the main sources for the solid material supply (Zhang et al., 2014; Liu et al., 2016; Yang et al., 2022), which is consistent with the assumptions of Dens-ID (Zhang et al., 2020). Thus, JJG is used as the study zone for deriving the function that describes the relationship between

110   AEP and P_{df}.

3 Methods and data

3.1 Dens-ID

Debris flow gullies characterized by a solid source supply from landslides are widely distributed in southwest China (Zhang et al., 2014). For this type of debris flow gully, our previous study proposed Dens-ID aiming at correlating debris-flow density to rainfall parameters based on water-soil coupling mechanism (Zhang et al., 2020; Long et al., 2020). Den-ID assumes debris flow to be a water-soil mixture, it contains three core simulating contents including hydrological simulation, water-soil coupling to calculate the water-soil-mixture density, and correlating density to rainfall parameters.

(1) Simulating hydrological process: the purpose is to provide parameters for estimating rainfall-induced runoff and the supply volume of rainfall-induced loose solid materials. Based on the digital elevation model (DEM) of a gully, Den-ID can simulate the rainfall-induced runoff and water diffusion in the vertical direction within the soil mass. The rainfall infiltration border is controlled by Equation 1.

$$-D(\theta)\frac{\partial \theta}{\partial z} + K(\theta) = I(t) \tag{1}$$

where θ is the soil water content; $D(\theta) = K(\theta)/(d\theta/d\psi)$, which represents the soil water diffusivity; z is the soil depth, which is positive downwards along the soil depth as the topsoil is taken as the origin point; $K(\theta)$ is the hydraulic conductivity; $I(t)$ is the rainfall intensity; and ψ is the soil matrix suction. When the rainfall intensity is less than the surface infiltration capacity, Equation 1 is used to represent this physical process; whereas the case of precipitation intensity exceeding the infiltration capacity of topsoil means that the surface is saturated, and the excess

132 precipitation from the topsoil is converted into runoff. Therefore, the pressure infiltration of each

133 grid cell is not considered.

134
$$\frac{\partial \theta}{\partial t} = \frac{\partial}{\partial z}[D(\theta)\frac{\partial \theta}{\partial z}] - \frac{\partial K(\theta)}{\partial z}$$
(2)

135 Equation 2 is the Richard differential infiltration equation (Richards, 1931), which is used to

136 describe the water movement along the vertical direction within soil mass after precipitation

137 infiltrates into topsoil. Dens-ID uses the finite-difference method to solve Eqs. 1 and 2 and can

138 provide the runoff depth (denoted as $dw(i,t)$), soil water content, and soil matrix suction for each

139 grid cell. Dens-ID then calculates the runoff volume using runoff depth $dw(i, t)$ in Equation 3.

140
$$V_w(t) = \sum_{t=1}^{T}\sum_{i=1}^{n} S_g * dw(i,t)$$
(3)

141 where n represents the total number of grid cells that can generate runoff at time t, $V_w(t)$ represents

142 the total volume of runoff within a gully at time t, S_g represents the area of the grid cell generating

143 runoff, and T represents the total duration of a rainfall process.

144   (2) Calculating supply amount of loose solid materials and density of the water-soil mixture:

145 taking hydrological parameters such as soil water content and soil matrix suction as inputs, Dens-

146 ID uses Equations 4 and 5 to estimate the supply amount of rainfall-induced loose solid materials

147 within a gully. Equation 4 calculates safety factor F_s of each grid cell as a function of the matrix

148 suction and soil moisture. $F_s > 1$ indicates that the grid cell is stable and cannot supply solid material

149 to the gully, whereas a grid with $F_s < 1$ can provide solid material in the form of a shallow landslide.

150
$$F_s = \frac{tan\,\varphi}{tan\,\beta} + \frac{c + \psi\,tan(\varphi^b)}{\gamma_t d_s\,cos\,\beta\,sin\,\beta}$$
(4)

151 where F_s represents the safety factor of each grid cell, c is the soil cohesion force, φ is the internal

152 friction angle, φ^b is related to the matrix suction and is approximately equal to φ as the low matrix

153 suction is small, d_s is the soil depth, and ψ is the matrix suction which is a function of soil water

154   content and can be described by the Van Genuchten model (Van Genuchten, 1980).

155   Equation 4 is used to estimate the total volume of solid materials from all the unstable grid

156   cells during a rainfall process.

157 $$V_s(t) = \sum_{t=1}^{T} \sum_{j=1}^{m} S_g * ds(j,t)$$ (5)

158   where m represents the number of grid cells that can provide solid material at time t and $V_s(t)$ is the

159   total volume of solid material within a gully at time t. At time t, the density of the water-soil mixture

160   after full coupling between runoff and solid material can be calculated using Equation 6.

161 $$\rho_{mix}(t) = \frac{\rho_w V_w(t) + \rho_s V_s(t)}{V_{mix}(t)}$$ (6)

162   where $\rho_{mix}(t)$ is the density of the water-soil mixture, ρ_w is the water density, ρ_s is the density of

163   the soil particles, and $V_{mix}(t)$ is the volume of the water-soil mixture, which is the sum of $V_w(t)$

164   and $V_s(t)$. $V_w(t)$ and $V_s(t)$ are the key variables that can be derived using Eqs. 3 and 5.

165   (3) Correlating density to rainfall parameters including rainfall intensity and duration: after

166   firstly presetting the density of the water-soil mixture as ρ_{mix}, Dens-ID also needs to simulate many

167   rainfall scenarios including long durations with low-intensity rainfall and short durations with high-

168   intensity rainfall in order to obtain a sufficient number of [D_i, l_i]. Using each [D_i, I_i] as input, Dens-

169   ID then can calculate the density using Equation 6. If the calculated density is equal to ρ_{mix}, the [D_i,

170   I_i] combination is saved by Dens-ID. After Dens-ID completes the trial calculations, all combination

171   data of [D_i, I_i] that satisfy the constraints of the preset density (ρ_{mix}) can be collected as a dataset.

172   Each collected [D_i, I_i] within the dataset corresponds to the preset ρ_{mix}, accordingly, Dens-ID can

173   correlate rainfall parameters (D and I) to debris flow density (Long et al., 2020). Dens-ID can derive

174   ID threshold curves by fitting the selected [D_i, I_i] data, and each ID curve corresponds to a debris

175   flow density value (Zhang et al., 2020). As the density of debris flow in JJG varies in a specific

176 interval of 1.2–2.3g/cm³ (Zhang et al., 2014; Zhuang et al., 2015; Long et al., 2020), the threshold

177 curve that corresponds to the boundary value can form a closed area with the I- and D-axes in the

178 ID coordinate system. The case of monitoring or forecasting rainfall falling into this closed area

179 indicates that the rainfall condition may trigger debris flow. The verification results in JJG show

180 that Dens-ID can effectively describe the mechanism and process of debris flow formation, and its

181 prediction accuracy is approximately 80.5%, which is 27.7% higher than that of statistical models

182 (Zhang et al., 2020). Such a high prediction accuracy can further indicate that the closed area formed

183 by the derived ID curves has a very reasonable location and coverage in the ID coordinate system,

184 providing extremely reliable analytical data in this study.

185 **3.2 JJG data for model Dens-ID**

186 The JJG datasets for Dens-ID are terrain data, hydrological parameters, and soil mechanical

187 parameters. The DEM is the basal data for deriving other terrain data, including slope length,

188 gradient, and river channels; the spatial resolution of the DEM is 0.5 m, and a DEM with a grid size

189 of 10 m was generated using the resampling technology in ArcGIS. The hydrological parameters

190 are related to the soil types within JJG; the five key parameters are the saturated soil water content,

191 residual soil water content, the two parameters of soil water characteristic curve including *n* and *m*,

192 and the infiltration rate of topsoil. The soil mechanical parameters are the soil cohesion force and

193 internal friction angle obtained through direct shear tests on the soil samples. Detailed data are

194 available in Zhang et al. (2020) and Long et al. (2020).

195 **3.3 Historical rainfall and debris flow data**

196   Rainfall data for the rainy seasons between 2006 and 2020 have been collected from the JJG

197   observation station, and it is necessary to identify each rainfall process from the long-term rainfall

198   sequences. Inter-event time (IET) is defined as the minimum time interval between two consecutive

199   rainfall pulses (Adams et al., 1986). IET has a strong influence on the rainfall event starting and

200   ending times (Bel et al., 2017), and Peres et al. (2018) has identified that IET depends on whether

201   the mean daily potential evapotranspiration (MDPE) is larger than precipitation within the IET. The

202   long observation of evaporation within JJG showed that MDPE is about 4 mm; precipitation during

203   IET >0.5 mm is considered the end of a rainfall process. Under this standard, 1094 rainfall events

204   and 37 debris flow events have been identified during the sampling period. Detailed rainfall data

205   information can be found in "appendix 1-1094 rainfall and 37 debris flow data.xlsx". The AEP listed

206   in this appendix is considered the weighted sum of the rainfall periods before the occurrence of

207   debris flow (Long et al., 2020) and it can be calculated using Equation 7.

$$AEP = \sum_{i=1}^{n} K^n R_i \tag{7}$$

209   where AEP is the antecedent effective rainfall; K is the attenuation coefficient, which is equal to

210   0.78 based on the field test in JJG (Zhang et al., 2020); and n is the number of days preceding the

211   debris flow occurrence.

212   Based on the observed rainfall data, the 1094 AEPs are calculated using Equation 7 and listed

213   in Appendix 1. The AEP corresponding to each rainfall event varies from 0–88 mm. Taking this

214   variation range as a reference, the variation range of the AEP input in the Dens-ID model is set

215   between 10 and 85 mm. Since AEP in JJG ranges in 0-88 mm according to the measured rainfall

216   data, Dens-ID presets several AEP values including 10, 15, 20, 25, 30, 35, 40, 45, 50, 55, 60, 65, 70,

217   75, 80, 85. The cases of AEP=0 and AEP=5 mm are excluded, because the two cases represents such

218 a low initial rainfall condition that any ID curve cannot derived from Dens-ID. The purpose of

219 increasing AEP by an interval of size 5 is to get adequate ID curves, which will be helpful to

220 calculate P_{df} under different AEP conditions.

221 **3.4 Monte Carlo method for calculating the definite integral**

222 Because of the boundary of the debris-flow density in JJG (1.2–2.3g/cm^3), Dens-ID produces

223 the corresponding upper and lower boundary curves under a specific AEP condition. The two

224 boundary curves can be described using the power function.

225
$$\begin{cases} f(D)_{up} = I_{up} = \alpha_1 D^{\beta_1} & D\epsilon[a_1,b_1] \\ f(D)_{low} = I_{low} = \alpha_2 D^{\beta_2} & D\epsilon[a_2,b_2] \end{cases} \tag{8}$$

226 These two threshold curves can delineate an enclosed area in the ID coordinate system, denoted

227 as W_{ID}. The independent variable (D) and dependent variable (I) in Equation 8 also form a closed

228 rectangular region in the ID coordinate system, denoted as R_{ID}. In the ID coordinate system, the

229 coverage of R_{ID} is larger than that of W_{ID}, as will be shown in detail in Section 4.1. Limited within

230 R_{ID}, any rainfall processes located in W_{ID} can trigger debris flow. If the probability of rainfall

231 process falling into the range of W_{ID} under random conditions is determined, the occurrence

232 probability of debris flow can be estimated. Many physical phenomena are stochastic in nature and

233 governed by stochastic partial differential equations with nondeterministic initial/boundary

234 conditions or integral equations (Peres and Cancelliere, 2014; Yan and Hong, 2014). Albert (1956)

235 proposed the Monte Carlo method for solving integral equations. This method is subsequently used

236 to estimate the peak flow and volume of debris flow (Donovan and Santi, 2017; Paola et al., 2017),

237 entrainment of the underlying bed sediment (Han et al., 2015), and risk assessment (Calvo and Savi,

238 2009; Li et al., 2021). The rainfall process is randomly selected within the R_{ID}, and the probability

239 of the chosen one falling into the W_{ID} can be determined using W_{ID}/R_{ID}. The physical meaning of

240 the Monte Carlo solving definite integral lies on calculating the area enclosed by the function curve

241 and horizontal axis. Therefore, the area of W_{ID} can be calculated by the difference in the definite

242 integral formula of the two equations in Equation 8.

243
$$W_{ID} = S_{up} - S_{low} = \int_{a1}^{b1} f(D)_{up} dD - \int_{a2}^{b2} f(D)_{low} dD \tag{9}$$

244 where S_{up} and S_{low} represent the area enclosed by the two threshold curves and the horizontal axis,

245 respectively, and a_1, b_1, a_2, and b_2 are the boundary values of D in the two curves. For the upper

246 boundary line (or lower boundary), if the probability distribution function of D between [a1, b1] is

247 p(D), Equation 10 can be derived by substituting p(D) into Equation 9.

248
$$\begin{cases} S_{up} = \int_{a_1}^{b_1} f(D)_{up} dD = \int_{a_1}^{b_1} \frac{f(D)_{up}}{p(D)} p(D) dD \approx \frac{1}{n} \sum_{k=1}^{n} \frac{f(D_i)_{up}}{p(D_i)} \\ S_{low} = \int_{a_2}^{b_2} f(D)_{low} dD = \int_{a_2}^{b_2} \frac{f(D)_{low}}{p(D)} p(D) dD \approx \frac{1}{n} \sum_{k=1}^{n} \frac{f(D_i)_{low}}{p(D_i)} \end{cases} \tag{10}$$

249
$$W_{ID} = \frac{1}{n} \sum_{k=1}^{n} \frac{f(D_i)_{up}}{p(D_i)} - \frac{1}{n} \sum_{k=1}^{n} \frac{f(D_i)_{low}}{p(D_i)} \tag{11}$$

250 where n represents the number of random samples drawn from the variation range of D, and $p(D_i)$

251 is the probability density distribution function of D in the interval $[a_1,b_1]$ or $[a_2,b_2]$. The key to

252 solving Equation 10 depends on sampling from p(D). The following steps are used to explain how

253 samples were taken using $p(D_i)$.

254 Step 1: Based on the probability density distribution function p(D), the cumulative probability

255 distribution function can be derived by cdf(D)$=\int_{-\infty}^{b} f(D) dD$;

256 Step 2: Assume that $U^{(i)}$ obeys a uniform distribution within [0,1], which can be randomly collected

257 from this interval and denoted as $U^{(i)} \sim U(0,1)$.

258 Step 3: Substitute $U^{(i)}$ into the inverse function of the cumulative probability distribution cdf(D) to

259 obtain random sample $D^{(i)}$, denoted by $D^{(i)} = cdf^{-1}(U^{(i)})$. Then, a dataset composed of n data

260 points of $D^{(i)}$ is obtained.

261   Step 4: W_{ID} can be calculated by substituting n data points of $D^{(i)}$ into Equation 10, and the P_{df}

262   ($P_{df} = \frac{R_{ID}}{W_{ID}}$) corresponding to a specific AEP is determined. P_{df} represents the probability that the

263   subsequent precipitation process may trigger debris flow for a certain AEP. Thus, the influence of

264   the AEP on the occurrence probability of debris flows can be quantified.

265   **3.5 Correlation analysis between numerical and observation results**

266   The relationship between the AEP-P_{df} fitted through the observational data is used as a

267   reference standard, and the correlation analysis method is used to verify the function of the AEP-P_{df}

268   derived by Dens-ID. Correlation analysis is used to study the degree of linear correlation between

269   variables, which is represented by correlation coefficient r:

270    $$r = \frac{\sum_{i=1}^{n}(x_i - \bar{x})(y_i - \bar{y})}{\sqrt{\sum_{i=1}^{n}(x_i - \bar{x})^2 \sum_{i=1}^{n}(y_i - \bar{y})^2}} \tag{12}$$

271   where x represents the P_{df} derived from the observed data, y represents the P_{df} derived from Dens-

272   ID, $\bar{x}$ and $\bar{y}$ represent the averages, r represents the correlation coefficient, and n represents the

273   number of samples. $|r| \geq 0.8$ can be regarded as a high correlation between two variables; $0.5 \leq |r| < 0.8$

274   represents a moderate correlation; $0.3 \leq |r| < 0.5$ represents a low correlation; and $|r| < 0.3$ indicates the

275   degree of correlation between the two variables is weak and can be regarded as uncorrelated.

276   **4 Results**

277   **4.1 ID threshold curves and warning zone closed by the derived curves**

278   Dens-ID yields the upper and lower boundary lines of the ID threshold in each condition of a

279   preset AEP, and these two boundary lines are characterized by different debris flow density and

280   listed in Table 1. It can be seen from Table 1 that the maximum density corresponding to the ID

281   threshold curve cannot reach 2.2, when AEP is less than 15 mm. A small AEP indicates the supply

282   rate of solid resources in JJG is far less than the runoff generation rate during a subsequent rainfall

process. In this situation, runoff is dominated in the water-soil coupling process yielding a water-soil mixture with low density value.

Table 1 ID threshold curve database under different AEP

AEP (mm)	ID threshold curve function for JJG	
	1.2 g/cm^3	2.2 g/cm^3
10	$I_{1.2} = 19.85D^{-0.54}$ D∈[1, 269] ($R^2 = 0.991$)	$I_{1.8}=15.85D^{-0.48}$ D∈[1, 263] ($R^2=0.990$)
15	$I_{1.2}= 21.69D^{-0.55}$ D∈[1, 236] ($R^2=0.993$)	$I_{2.0}=16.10D^{-0.50}$ D∈[1, 229] ($R^2=0.995$)
20	$I_{1.2}=23.22D^{-0.58}$ D∈[1, 203] ($R^2=0.996$)	$I_{2.2}=17.20D^{-0.53}$ D∈[1, 192] ($R^2=0.995$)
25	$I_{1.2}=24.47D^{-0.60}$ D∈[1, 171] ($R^2=0.997$)	$I_{2.2}=16.92D^{-0.53}$ D∈[1, 160] ($R^2=0.998$)
30	$I_{1.2}=26.24D^{-0.64}$ D∈[1, 143] ($R^2=0.996$)	$I_{2.2}= 18.09D^{-0.57}$ D∈[1, 132] ($R^2=0.995$)
35	$I_{1.2}=35.47D^{-0.65}$ D∈[1, 123] ($R^2=0.958$)	$I_{2.2}= 19.55D^{-0.58}$ D∈[1, 112] ($R^2=0.985$)
40	$I_{1.2}= 40.59D^{-0.78}$ D∈[1, 103] ($R^2=0.966$)	$I_{2.2}= 22.15D^{-0.64}$ D∈[1, 92] ($R^2=0.984$)
45	$I_{1.2}= 41.12D^{-0.78}$ D∈[1, 83] ($R^2=0.932$)	$I_{2.2}= 23.19D^{-0.69}$ D∈[1, 72] ($R^2=0.981$)
50	$I_{1.2}=41.26D^{-0.86}$ D∈[1, 65] ($R^2=0.981$)	$I_{2.2}= 23.50D^{-0.74}$ D∈[1, 55] ($R^2=0.980$)
55	$I_{1.2}=38.63D^{-0.88}$ D∈[1, 53] ($R^2=0.950$)	$I_{2.2}= 23.31D^{-0.70}$ D∈[1, 42] ($R^2=0.932$)
60	$I_{1.2}= 31.49D^{-0.92}$ D∈[1, 40] ($R^2=0.992$)	$I_{2.2}= 20.73D^{-0.86}$ D∈[1, 30] ($R^2=0.977$)
65	$I_{1.2}= 29.14D^{-0.95}$ D∈[1, 32] ($R^2=0.957$)	$I_{2.2}= 18.10D^{-0.91}$ D∈[1, 22] ($R^2=0.893$)
70	$I_{1.2}= 23.05D^{-0.96}$ D∈[1, 25] ($R^2=0.998$)	$I_{2.2}= 13.04D^{-0.93}$ D∈[1, 15] ($R^2=0.995$)
75	$I_{1.2}= 21.13D^{-0.97}$ D∈[1, 22] ($R^2=0.994$)	$I_{2.2}=10.90D^{-0.95}$ D∈[1, 12] ($R^2=0.995$)
80	$I_{1.2}= 18.72D^{-0.98}$ D∈[1, 20] ($R^2=0.997$)	$I_{2.2}= 9.96D^{-0.95}$ D∈[1, 11] ($R^2=0.999$)
85	$I_{1.2}= 18.47D^{-0.99}$ D∈[1, 18] ($R^2=0.999$)	$I_{2.2}= 8.17D^{-0.95}$ D∈[1, 9] ($R^2=0.999$)

Under the condition of AEP < 10 mm, Dens-ID cannot derive the threshold curve corresponding to even the minimum density value of 1.2 g/cm^3, which indicates that the subsequent rainfall can hardly trigger debris flow JJG. Table 1 also shows that the AEP ranging from 10 to 85 mm can significantly affect the ID threshold curve, because the parameters including α and β regularly respond to the change in AEP.
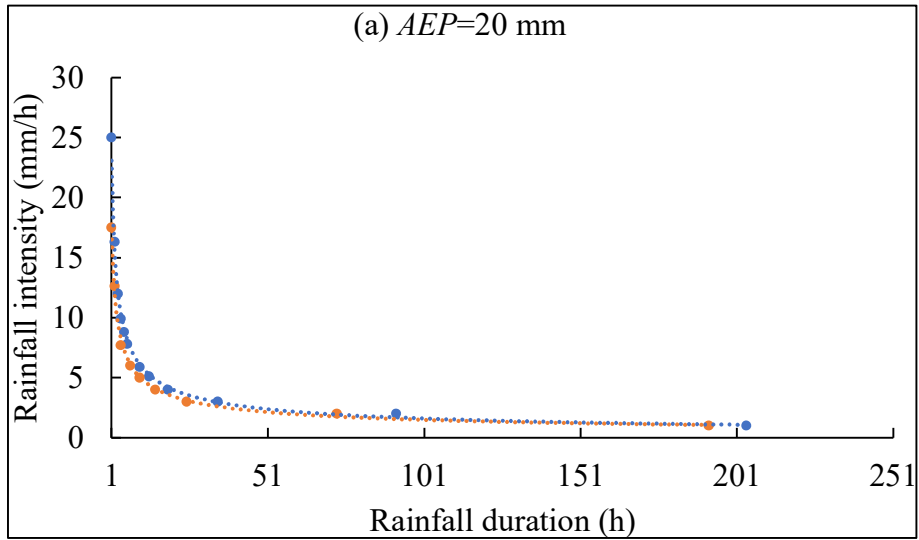
291
292
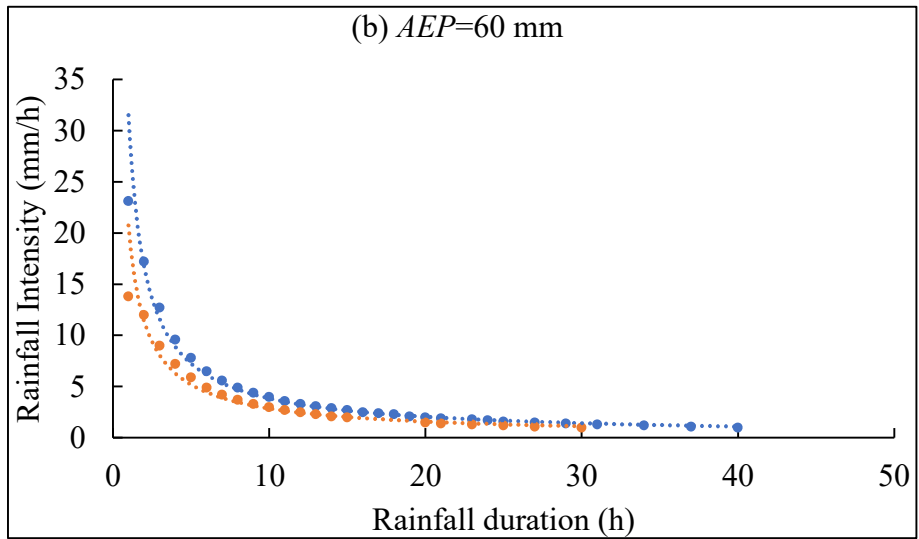
293
294
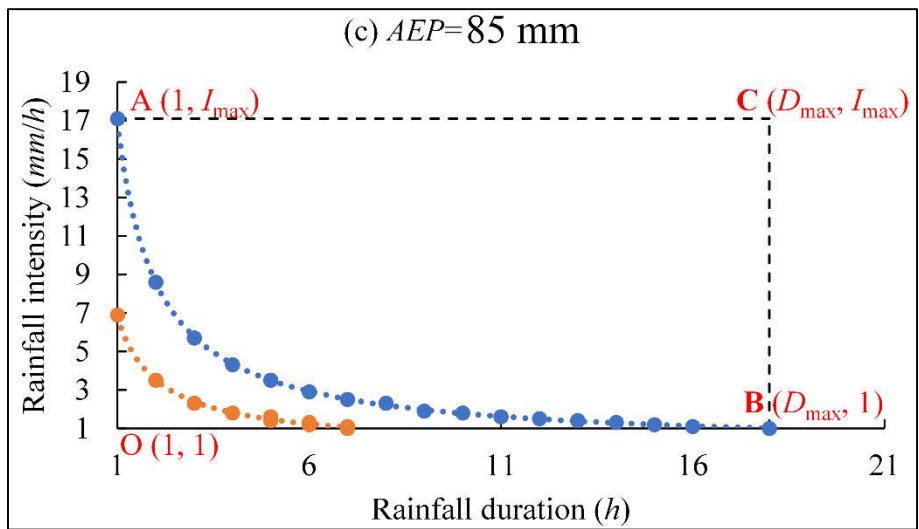
295

296   Fig.2 ID threshold curves derived by Dens-ID (the blue dotted line corresponds to 1.2 g/cm³, and

297   the orange dotted line corresponds to 2.2 g/cm^3)

298   There are two ID threshold curves in each subplot of Fig. 2, which correspond to 1.2 g/cm^3 and

299 2.2 g/cm^3, respectively. Because the debris flow density in JJG varies within a certain range from

300 1.2–2.3 g/cm^3, the two ID threshold curves shown in each subplot can be regarded as the upper and

301 lower boundary lines for determining the occurrence of debris flow (Zhang et al., 2020). Within the

302 ID coordinate system, the two derived curves together with the I- and D-axes delineate a closed area

303 shown in Fig.2c. Any subsequence rainfall represented by the combination of I and D falling into

304 W_{ID} may trigger a debris flow. As shown in each subplot, the threshold curve can be represented by

305 the power function $I=\alpha D^\beta$. The variation intervals of the independent (D) and dependent (I) variables

306 of the power function are [1, D_{max}] and [1, I_{max}], respectively, where D_{max} represents the rainfall

307 duration required to trigger debris flow when I= 1 mm/h, and I_{max} represents the rainfall intensity

308 required for debris flow formation for D=1 h. As shown in Fig.2c, independent variable D and

309 dependent variable I can delineate a larger rectangular area (AOBC) in the ID plane than W_{ID}, which

310 is denoted as R_{ID}. The coverage area of R_{ID} is much larger than that of W_{ID} indicating that the

311 proportion of rainfall conditions that can trigger debris flows is low. Therefore, even for AEP=85

312 mm, the occurrence probability of debris flows remains low. As shown in each subplot, each AEP

313 corresponds to a different W_{ID} and R_{ID}, which provides basic data for the quantitative evaluation of

314 the effect of different AEPs on the occurrence probability of debris flows.

315 **4.2 Occurrence probability of debris flow under different AEP**

316   Based on the Monte Carlo method of calculating the definite integral, it is necessary to explore

317 the probability density function of rainfall duration (D) to calculate the occurrence probability of

318 debris flow under different AEP conditions. For the 1094 rainfall events listed in Appendix 1, we

319 found that the probability distribution of rainfall duration D in JJG can be described by a power

320 function (Fig. 3). As shown in Fig.3, the number of samples with D<1 accounted for 37.7%, 1<D<3

321 for 23.5%, 3<D<5 for 14.7%, and 5<D<10 for 16.9%; the number of rainfall events with D

322 exceeding 10 h accounted for only 6.7%.
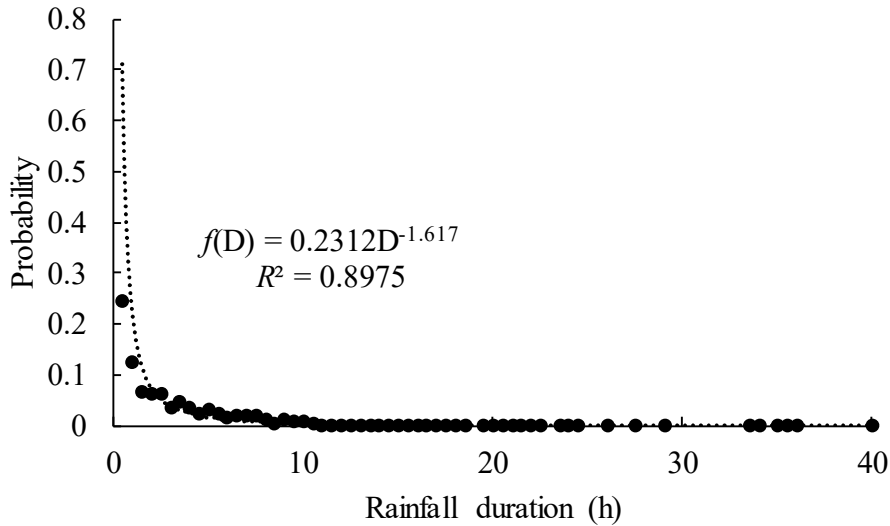
323

324 Fig. 3 Probability density function of f(D)

325 Based on the probability density distribution function f(D)=0.2312D$^{-1.617}$, the cumulative

326 probability function cdf(D) can be obtained through integration. In cdf(D), denoted as Equation 13,

327 the integration constant C needs to be determined.

$$cdf(D)= \int_{-\infty}^{D} f(D)dD=\text{-}0.3747\text{*}D^{-0.617}+C \qquad (13)$$

329 The range of 0–40 h is evenly divided into 56 statistical intervals (the second column in

330 Appendix 2, titled "appendix 2-f(D)and CFD(D). xlsx"), and each statistical interval is separated by

331 0.5 h. The proportion of the sample size in each interval among the 1094 samples can be calculated

332 and listed in the second column in Appendix 2; the cumulative proportion that increases with D is

333 also derived and listed in the third column in Appendix 2. The data in the first and third columns of

334 Appendix 2 are substituted into Equation 13 to calculate C. The results show that C increases with

335 D but gradually stabilizes at approximately 1.04 (the fifth column in Appendix 2). Therefore, C is

336   set to 1.04.

337   Based on the process of calculating P_{df} under different AEP conditions in Section 3.4, the P_{df}

338   corresponding to each AEP in Table 1 is obtained, and the function $P_{df} = f(AEP)$ for describing

339   their relationship has been fitted using the AEP and P_{df} data.

$$P_{df} = 0.3442e^{0.0457AEP} \tag{14}$$

341   As shown in Equation14, the relationship of AEP and P_{df} obeys the rule of exponential function

342   as AEP changes from 10 to 85 mm, whereas $P_{df} = 0$ when AEP is less than 10 mm. The evolution

343   of P_{df} with AEP variation can be divided into two stages (Fig. 4). Two key issues must be stated

344   before discussing the two stages in depth: (1) Based on the calculation results of the Dens-ID model,

345   an upper limit volume of the rainfall-induced solid material supply is derived in JJG, which is the

346   basic condition for determining the scale of debris flow in JJG (Zhang et al., 2020). (2) Based on

347   the principle of water balance, AEP is defined as the rainfall that is preserved in the soil before the

348   triggering rainfall process (Kohler and Linsley, 1951); field observations in JJG show that the AEP

349   is positively correlated with the soil water content (Cui et al., 2007), and the field observations of

350   the Liudaogou catchment in the northern Loess Plateau of China have the same result (Zhu and

351   Shao, 2008); therefore, the AEP is typically used to estimate soil water content (Crozier, 1986; Chen

352   et al., 2018; Zhao et al., 2019b). The water soil content before the triggering rainfall process can be

353   characterized by AEP (Thomas et al., 2019; Schoener and Stone, 2020).

$$P_{df} = 0.3442e^{0.0457AEP}$$
$$R^2 = 0.9707$$
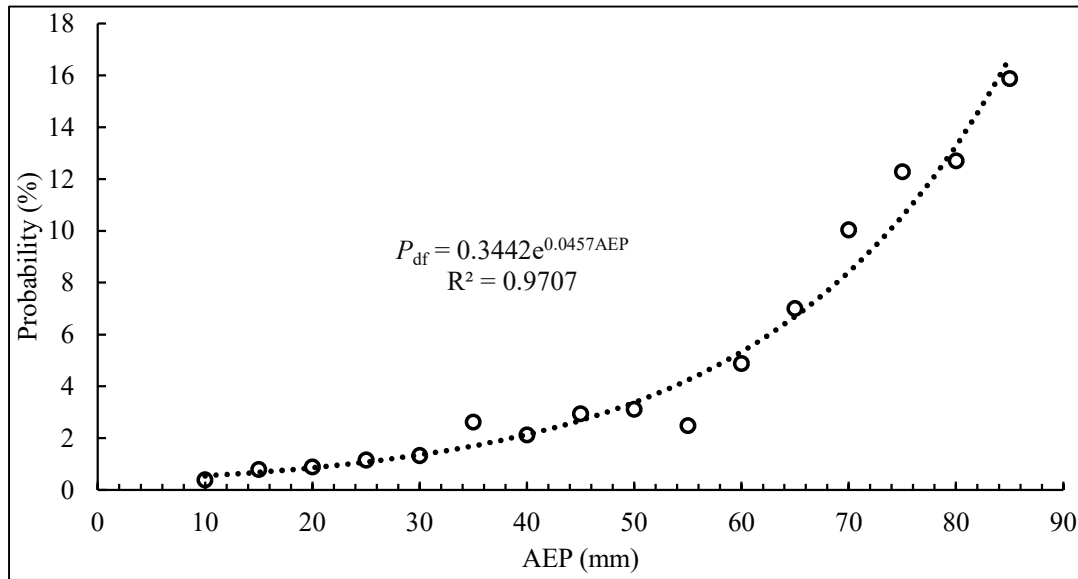
Fig.4 Relationship of P_{df} and AEP derived from Dens-ID

Stage 1: The probability of debris flow occurrence in JJG is equal to 0 when the AEP is < 10

mm. Dens-ID estimates the solid material volume by simulating rainfall-induced shallow landslides.

According to Equation 4, the key hydrological process that triggers shallow landslides is the

continuous increase in soil water content caused by rainfall infiltration. The increase in soil moisture

content reduces soil matrix suction and eventually contributes to shallow landslides. The soil water

content of the loose soil mass in JJG is low when the AEP < 10 mm (Long et al., 2020), and a long

duration of rainfall infiltration is needed to increase the soil water content. However, based on the

infiltration border of Dens-ID (Equation 1), limited by the infiltration capacity of the topsoil in JJG,

the portion of precipitation that exceeds the infiltration capacity is be converted into runoff;

therefore, when the water content of the soil layer in JJG is low, the surface runoff can be rapidly

generated. Therefore, the runoff generation rate can be much higher than the supply rate of solid

material in the condition of AEP < 10 mm. In this hydrological scenario, Dens-ID determines that

even a soil-water mixture with a density of 1.2 g/cm^3 is difficult to generate in JJG; thus, the

probability of debris flow is 0.

370   Stage 2: When AEP varies within the interval of 10 mm-85mm, the subsequent rainfall is

371   capable of triggering debris flow in JJG. Compared to AEP < 10 mm in Stage 1, the soil water

372   content within JJG increased significantly. Therefore, the solid material from shallow landslides can

373   be immediately ready without a long rainfall infiltration duration, and a large water content of

374   topsoil is beneficial to the rapid generation of runoff (Jones et al., 2017; Hirschberg et al., 2021).

375   When there is a sufficient supply of solid material and runoff, the probability of debris flow

376   occurrence in Stage 2 is significantly increased by the increasing AEP. The relationship between

377    $P_{df} \sim AEP$ can be described by an exponential function of $P_{df}=0.3442e^{0.0457AEP}$. The exponential

378   function and its boundary show that the increasing tendency of P_{df} is a little sluggish before AEP is

379   equal to 50 mm. The occurrence probability of debris flow in JJG is only 15.88% even when AEP

380   is equal to 85 mm.

381   **5 Discussions**

382   **5.1 Correlation analysis of the two curves derived from Dens-ID and observation data**

383   The AEP in Appendix 1 varied from 0–87.9 mm, according to this range, we can test the

384   reasonability of the relationship between $P_{df} \sim AEP$ shown in Fig. 4. We introduce how to use the

385   rainfall and debris flow data recorded in Appendix 1 to calculate P_{df}: (1) The original AEP value is

386   rounded to one decimal place, and the rounded AEP are listed in the 8th column of Appendix 1,

387   which were sorted from largest to smallest; (2) the maximum AEP_i was set to 85 mm, and [AEP_i,

388   AEP_i-5] was used as the search window to collect the rainfall events and debris flow events; and (3)

389   we count the number of debris flow events N_{df} and the number of rainfall events N_{rain} in each search

390   window and then calculate $P_{df}=N_{df}/N_{rain}$. Based on the above steps, the collected data and calculated

391   P_{df} are listed in Table 2. As shown in Table 2, a positive correlation between the probability of debris

392   flow occurrence and AEP in JJG was determined. When AEP < 10 mm, a total of 205 rainfall

393   processes were recorded; however, no debris flow events were observed, and the debris flow

394   occurrence probability was 0, which is consistent with the results of Stage 1 derived from Dens-ID.

395   Table 2 Collected and calculated P_{df} in each search window

	Field observation data and calculated P_{df}										
AEP	10	15	20	25	30	35	40	45	50	75	80
N_{df}	0	3	2	7	7	4	4	5	3	1	1
N_{rain}	205	133	111	127	124	106	106	49	31	8	5
P_{df} (%)	0	2.3	1.8	5.5	5.6	3.8	3.8	10.2	9.7	12.5	20

396   Based on P_{df} and AEP listed in Table 2, their relationship can be described by the exponential

397   function denoted as $P_{df} = 1.5917e^{0.031AEP}$, which is similar to Equation14 drawn in Fig.4. The

398   two curves were nearly parallel. Equation 12 was used to analyze the correlation of the two curves,

399   and *r* is equal to 0.93, suggesting they have a very high correlation. Therefore, the function of $P_{df} =$

400    $f(AEP)$ derived from Dens-ID, which is used to describe the evolution trend of debris flow

401   occurrence probability with AEP variation, is reasonable.
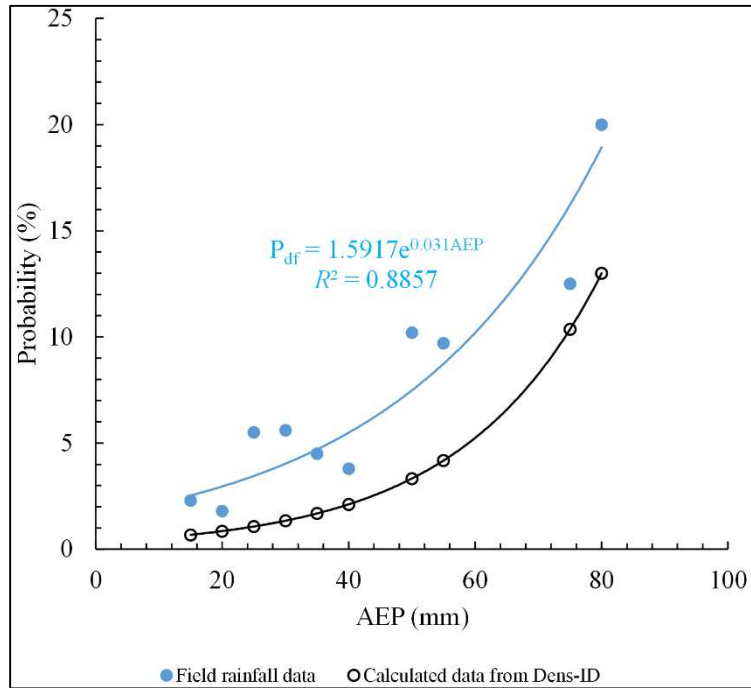
Fig.5 Relationship of AEP and P_{df} obtained from field observation data and Dens-ID model (the blue line is

derived from field observation data, and the black line is derived from Dens-ID)

We can also see from Fig.5 that although the variation tendencies of the two curves are

consistent, a significant bias existed between them. Basically, the probability value derived from the

field observation data is larger than that from the Dens-ID model in the condition of a given AEP.

As shown in Fig.5, the blue line fitted through the observation data is above the black line derived

from Dens-ID, indicating that Dens-ID underestimated the probability of debris flow occurrence if

the observation data were used as the reference. Taking the probability value in the 6th row of Table

2 as references, the error of the Equation14 was calculated using the AEP in Table 2 as inputs and

listed in Table 3.

Table 3 Error estimation on the Equation 14

AEP	15	20	25	30	35	40	45	50	75	80
Error	0.70	0.53	0.81	0.76	0.63	0.44	0.67	0.57	0.17	0.35

It can be seen that very large bias of Equation12 is listed in Table 2. However, we cannot

415 conclude that there is a precision problem in the calculation results of the Dens-ID. Because (1)

416 Although 1094 rainfall processes and 37 debris flow events are the field observation data, there are

417 many uncertain factors in Equation 7 for calculating AEP using these rainfall data (Kim et al., 2021),

418 such as the subjectivity existing in K and n of Equation 7, which render uncertainty in the calculated

419 AEP. In this case, if the data in Appendix 1 are used as the real value for evaluating the precision of

420 Dens-ID, the error evaluation result may be unfair to Dens-ID. In this case, it is unfair to evaluate

421 the Dens-ID error by using the calculated AEP in Appendix 1 as the true value. However, this

422 uncertainty can show consistent directional deviations because of the fixed values of K and n in

423 Equation 7; therefore, the uncertainty has no effect on the correlation analysis. (2) To establish the

424 functional relationship between P_{df}-AEP, many rainfall scenarios were simulated using the Dens-ID

425 model. Dens-ID simulated 3376, 3182, 2677, and 2677 rainfall processes with AEP = 20, 40, 45,

426 and 50 mm, respectively. The total number of simulated rainfall processes was significantly larger

427 than that of the 1094 observed rainfall events. The collected 1094 rainfall events still cannot fully

428 reflect all rainfall conditions in nature; that is, the amount of the observed 1094 rainfall data is still

429 inadequate when used as the denominator for calculating the probability of debris flow occurrence

430 in JJG. Therefore, the P_{df} calculated using the field observation data may be generally higher than

431 that calculated using Dens-ID. With the accumulation of rainfall observation data of JJG, it is

432 believed that the Pdf derived from field observation data will gradually decrease until it is close to

433 the calculated value of Dens-ID model. (3) Dens-ID cannot fully and accurately describe the

434 formation process of the debris flow in JJG because of the simplification in theory and boundaries.

435 Dens-ID is also affected by the accuracy of the input parameters (Zhang et al., 2020), which may

436 eventually lead to deviations between the simulation results and field observations.

437   5.2 Potential application and limitation

438   Deriving a quantified functional relationship of P_{df} and AEP would be more conducive to

439   examining the correspondence between these two parameters. Using mathematical physics method,

440   the function of $P_{df} = f(AEP)$ was firstly derived which can help us to learn more from the derived

441    $P_{df} = f(AEP)$.

442   Firstly, AEP is indeed an important factor affecting debris flow. Generally, there is the

443   following consensus in the field of debris flow: the greater the AEP, the higher the probability (P_{df})

444   of subsequent rainfall triggering the debris flow (De Vita et al., 2000; Bel et al., 2017). However,

445   this fuzzy qualitative description cannot explain the influence degree of AEP on the probability of

446   debris flow induced by subsequent rainfall. It can be seen from $P_{df} = f(AEP)$ that there are two

447   key value nodes of AEP affecting P_{df}: (1) point 10 mm:the case of AEP < 10 mm indicates that

448   any subsequent rainfall cannot trigger debris flow in JJG. Because the supply rate of solid material

449   is much lower than the runoff generation rate during subsequent rainfall in JJG, the water-soil

450   mixture within tends to be a hyperconcentrated flow rather than a debris flow (Long et al., 2020);

451   (2) Point 50 mm: the case of 10 mm≤AEP≤50 mm means that the soil water content increases

452   significantly compared to AEP < 10 mm, but a necessary infiltration time to increase it to the critical

453   state for triggering shallow landslides is still required. Therefore, limited by the supply rate of the

454   solid material, the increasing rate of P_{df} is sluggish. The case of 50 mm<AEP≤85 mm represents

455   the soil water content is relatively larger, the solid material from shallow landslides can be

456   immediately ready without a long rainfall infiltration duration, and a large soil water content of

457   topsoil is beneficial to the rapid generation of runoff (Jones et al., 2017; Hirschberg et al., 2021).

458   When there is a sufficient supply of provenance and runoff, the probability of debris flow occurrence

459   in this subprocess is significantly enhanced by the increasing AEP.

460   Secondly, Rainfall-induced debris flow is a small probability event compared with the rainfall

461   frequency in nature. JJG is well-known due to its high-frequency debris flow event. However, the

462   formation probability of debris flow in JJG induced by subsequence rainfall is only 15.88% even

463   the AEP reaches to 85 mm. Therefore, debris flow induced by rainfall in JJG is a small probability

464   event compared with the rainfall frequency. The figure of 15.88% means that the efficiency of rain-

465   induced debris flow is extremely low, which also indicates that the formation of debris flow is an

466   extremely complex physical process, in which rainfall is only one of the motivating factors, and

467   there are other more important internal factors affecting the formation of debris flow, such as

468   topography, source recharge and fluid characteristics of debris flow (Zhang et al., 2020). Thirdly, in

469   practical application, when the AEP in JJG is calculated according to Equation 7, the derived

470   exponential function can help us to assess the probability of debris flow in JJG triggered by

471   subsequent rainfall, according to which debris flow warning information can be issued in advance

472   to provide technical support for disaster prevention and reduction.

473   Our study also has its own limitations and needs to be listed for providing directions for

474   subsequent investigation. (1) Long-term observation data should be used to deduce the functions of

475    $P_{df} = f(AEP)$, however, the number of debris flow gullies with long-term observational data

476   worldwide is less than 10 (Hürlimann et al., 2019), accordingly, the function of $P_{df} = f(AEP)$

477   cannot yet be derived in other debris-flow gullies. (2) Dens-ID model assumes that the solid

478   material mainly comes from shallow landslides. However, the formation mechanism and solid

479   source supply mode of runoff-induced debris flow are different. Therefore, the functional of $P_{df} =$

480    $f(AEP)$for runoff-induced debris flow still needs to be studied with the help of other physical

481   models. (3) The calculation result of $P_{df} = f(AEP)$ derived from Dens-ID model has a large bias

482   from the observation data, the authors think that the main reason is insufficient field observation

483   data especially inadequate rainfall data. Basically, even for high-frequency debris flow gullies like

484   JJG, the success rate of debris flow induced by rainfall is still very low. Continuous increase of

485   rainfall and debris flow observation data will make the growth rate of Nrain in Table 2 much higher

486   than that of Ndf. Therefore, with the accumulation of rainfall observation data of JJG, it is believed

487   that the P_{df} derived from field observation data will gradually decrease until it is close to the

488   calculated result of Dens-ID model. Therefore, the authors will continue to collect field observation

489   data of JJG in the later period, and constantly verify the accuracy of Equation14 derived from Dens-

490   ID.

491   **5 Conclusions**

492   The Dens-ID model and Monte Carlo integral equation is used to derive function of $P_{df} =$

493    $f(AEP)$. The functional relationship is verified using a large amount of field observation data from

494   JJG. The following conclusions are drawn as follows.

495   The positive relationship between P_{df} and AEP is now described by a clear mathematical

496   equation in this study. the effective range of AEP that can affect debris flow formation verifies within

497   10–85 mm. Based on the simulation results, the probability of debris flow occurrence in JJG is 0 in

498   the condition of AEP < 10 mm, and the relationship between P_{df} and AEP can be described by an

499   exponential function when 10 mm≤AEP≤85 mm. The plausibility of the first two evolution stages

500   of the P_{df}-AEP piecewise function is effectively confirmed by the field observation data because the

501   P_{df}-AEP relationship obtained from field observation data is highly correlated with the simulation

502   results of Dens-ID. However, the reasonability of the last two stages of the P_{df}-AEP piecewise

503 function cannot be tested because of the lack of field observation data, and the errors of the P_{df}-AEP

504 piecewise function cannot be verified because of the uncertainty of the AEP derived from the

505 observation rainfall data.

506  This study mathematically confirms that "the greater the AEP, the higher the probability of

507 subsequent rainfall triggering debris flow" and quantifies this qualitative conclusion using piecewise

508 functions. This can effectively reveal the essential relationship between the two natural events of

509 rainfall and debris flow, quantitatively describe the impact of different AEPs on the probability of

510 debris flow occurrence, and provide key technical support for the early warning of debris flows.

511 **Code/Data availability**

512 Some or all data, models, or code generated or used during the study are available from the

513 corresponding author by request.

514 **Author Contribution**

515 SJZ, XHL, HJY, JM, and DLL conceptualized the work; developed the methodology; and carried

516 out the data curation, formal analysis, validation, and writing of the original draft. FQW and KHH

517 reviewed the initial manuscript.

518 **Competing interests**

519 The contact author has declared that none of the authors has any competing interests.

520 **Acknowledgement**:

521 This work was supported by the National Key Research and Development Program of China

522 (2023YFC3007205), the West Light Foundation of The Chinese Academy of Science, National

523 Natural Science Foundation of China (No. 42271013, No. 42001100), Project of the Department of

524 Science and Technology of Sichuan Province (No. 2023ZHCG0012).

References

Abraham, M.T., Satyan, N., Rosi, A., Pradhan, B., Segoni, S.: Usage of antecedent soil moisture for improving the performance of rainfall thresholds for landslide early warning. Catena, 200, 105147, 2021.

Abraham, M.T., Satyam, N., Pradhan, B., Alamri, A.M.: Forecasting of landslides using rainfall severity and soil wetness: A probabilistic approach for Darjeeling Himalayas. Water (Switzerland) 12, 1–19, 2020.

Adams, B., Fraser, H., Howard, C., Hanafy, M.: Meteorological data analysis for drainage system design. J. Environ. Eng. 112, 1986.

Albert, G.E.: A general theory of stochastic estimates of the Neumann series for solution of certain Fredholm integral equations and related series, in: M.A. Meyer (Ed.), Symposium of Monte Carlo Methods, Wiley, New York, 1956.

Bel, C., Liébault, F., Navratil O., Eckert N., Bellot H., Fontaine, F., Laigle, D.: Rainfall control of debris-flow triggering in the Réal Torrent, Southern French Prealphs, 291, 17-32, 2017.

Bennett, G.L., Molnar, P., Mcardell, B.W., Burlando, P.: A probabilistic sediment cascade model of sediment transfer in the Illgraben. Water Resources Research, 50, 1225-1244, 2014.

Bernard, M., Gregoretti, C.: The use of rain gauge measurements and radar data for the model-based prediction of runoff-generated debris flow occurrence in early warning systems. Water Resources Research, 57, e2020WR027893, 2021.

Berti, M., Simoni, A.: Experimental evidences and numerical modelling of debris flow initiated by channel runoff. Landslides, 3, 171-182, 2005.

Calvo, B., Savi, F.: A real-world application of Monte Carlo procedure for debris flow risk

547   assessment, Computers and Geosciences, 35(5), 967-977, 2009.

548   Castillo, V.M., Gómez-Plaza, A., Martínez-Mena, M.: The role of antecedent soil water content in

549   the runoff response of semiarid catchments: a simulation approach. Journal of Hydrology, 284,

550   114-130, 2003.

551   Chen, C.W., Oguchi, T., Chen, H., Lin, G.W. Estimation of the antecedent rainfall period for mass

552   movements in Taiwan, Environmental Earth Sciences, 77, 184, 2018.

553   Chen, C.W., Saito, H., Oguchi, T.: Analyzing rainfall-induced mass movements in Taiwan using the

554   soil water index, Landslides, 14, 1031-1041, 2017.

555   Coe, J.A., Kinner, D.A., Godt, J.W. Initiation conditions for debris flows generated by runoff at

556   Chalk Cliffs, central Colorado. Geomorphology, 3, 270-297, 2008.

557   Crozier, M.J.: Landslides: causes, consequences & environment. Croom Helm, London, p 25, 1986.

558   Cui, P., Zhu, Y.Y., Chen, J., Han, Y.S., Liu, H.J.: Relationships between antecedent rainfall and

559   debris flows in Jiangjia Ravine, China. In: Chen & Major, eds., Debris-Flow Hazards Mitigation:

560   Mechanics, Prediction, and Assessment, Millpress, Netherlands, 3-10, 2007.

561   De Vita, P.: Fenomeni d'instabilita` delle coperture piroclastiche dei Monti Lattari, di Sarno e di

562   Salerno (Campania) ed analisi degli eventi pluviometrici determinanti. Quad. Geol. Appl., 7, 213–

563   239, 2000.

564   Donovan, I.P., Santi, P.M. A probabilistic approach to post-wildfire debris-flow volume modeling,

565   Landslides, 14(4): 1345-1360, 2017.

566   Fiorillo, F., Wilson, R.C. Rainfall induced debris flows in pyroclastic deposits, Campania (southern

567   Italy). Engineering Geology, 75, 263-289, 2004.

568   Gabet, E.J., Mudd, S.M.: The mobilization of debris flows from shallow landslides. Geomorphology

569   1, 207-218, 2006.

570   Han, Z., Chen, G.Q., Li, Y.G., He, Y.: Assessing entrainment of bed material in a debris-flow event:

571   a theoretical approach incorporating Monte Carlo method: Assessing Entrainment of Bed

572   Material by Debris Flow, Earth surface processes and landforms, 40(14): 1877-1890, 2015.

573   Hirschberg, J., Badoux, A., McArdell, B.W., Leonarduzzi, E., Molnar, P.: Evaluating methods for

574   debris-flow prediction based on rainfall in an Alpine catchment. Nat. Hazards Earth Syst. Sci.,

575   21, 2773-2789, 2021.

576   Hong, M., Kim, J., Jeong, S.: Rainfall intensity-duration thresholds for landslide prediction in South

577   Korea by considering the effects of antecedent rainfall. Landslides, 15, 523–534, 2018.

578   Hu, W., Xu, Q., Wang, G.H., van Asch, T.W.J., Hicher, P.Y.: Sensitivity of the initiation of debris

579   flow to initial soil moisture. Landslides 12, 1139–1145, 2015.

580   Huang, C.H.: Critical rainfall for typhoon-induced debris flows in the Western Foothills, Taiwan.

581   Geomorphology, 185, 87-95, 2013.

582   Hürlimann, M. Coviello, V., Bel, C., Guo, X.J., Berti, M., Graf, C., Hübl, J., Miyata, S., Smith, J.B.,

583   Yin, H.Y.: Debris-flow monitoring and warning, Review and examples. Earth-Science Reviews,

584   199, 102981, 2019.

585   Iverson, R. M., Reid, M. E., LaHusen, R. G.: Debris Flow Mobilization from Landslides. Annu. Rev.

586   Earth Planet, 25: 85-138, 1997.

587   Jones, R., Thomas, R.E., Peakall, J., Manville, V.: Rainfall-runoff properties of tephra: Simulated

588   effects of grain-size and antecedent rainfall. Geomorphology, 282, 39-51, 2017.

589   Kim, S.W., Chun, K.W., Kim, M., Catani, F., Choi, B., Seo, J.: Effect of antecedent rainfall

590   conditions and their variations on shallow landslide-triggering rainfall thresholds in South Korea.

591 Landslides, 18, 569-582, 2021.

592 Kohler, M.A., Linsley, R.K.: Predicting the runoff from Storm Rainfall. US Department of

593 Commerce, Weather Bureau, Washington, D.C, 1951.

594 Le Bissonnais, Y., Renaux, B., Delouche, H. Interactions between soil properties and moisture

595 content in crust formation, runoff and interrill erosion from tilled loess soils. Catena, 25(1), 33-

596 46, 1995.

597 Li, L., Zhang, S.X., Li, S.H., Qiang, Y., Zheng, Z., Zhao, D.S.: Debris Flow Risk Assessment

598 Method Based on Combination Weight of Probability Analysis, Advances in civil engineering,

599 2021, 1-12, 2021.

600 Liu, D.L., Zhang, S.J., Yang, H.J., Zhao, L.Q., Jiang, Y.H., Tang, D., Leng, X.P.: Application and

601 analysis of debris-flow early warning system in Wenchuan earthquake-affected area. Nat. Hazards

602 Earth Syst. Sci., 16, 483-496, 2016.

603 Liu, X.L., Wang, F., Nawnit, K., Lv, X.F., Wang, S.J. Experimental study on debris flow initiation.

604 Bulletin of Engineering Geology and the Environment, 79, 1565-1580, 2020.

605 Long, K., Zhang, S.J., Wei, F.Q., Hu, K.H., Zhang, Q., Luo, Y. A hydrology-process based method

606 for correlating debris flow density to rainfall parameter and its application on debris flow

607 prediction. Journal of Hydrology, 589, 125124, 2020.

608 Luk, S.H.: Effect of antecedent soil moisture content on rainwash erosion. Catena, 12, 129-139,

609 1985.

610 Marra, F., Destro, E., Nikolopoulos, E.I., Zoccatelli, D., Creutin, J.D., Guzzetti, F., Borga, M.:

611 Impact of rainfall spatial aggregation on the identification of debris flow occurrence thresholds.

612 Hydrol. Earth Syst. Sci., 21, 4525-4532, 2017.

613   Paola, F.De., Risi, R.De., Crescenzo, G. Di, Giugni, M., Santo, A., Speranza, G.: Probabilistic

614   Assessment of Debris Flow Peak Discharge by Monte Carlo Simulation, Journal of Risk and

615   Uncertainty in Engineering Systems, Part A: Civil Engineering, 3(1), A4015002, 2017.

616   Papa, M.N., Medina, V., Ciervo, F., Bateman, A.: Derivation of critical rainfall thresholds for

617   shallow landslides as a tool for debris flow early warning systems. Hydrol. Earth Syst. Sci. 17,

618   4095-4107, 2013.

619   Peres, D.J., Cancelliere, A.: Derivation and evaluation of landslide-triggering thresholds by a Monte

620   Carlo approach. Hydrol. Earth Syst. Sci., 18, 4913-4931, 2014.

621   Peres, D.J., Cancelliere, A.: Modeling impacts of climate change on return period of landslide

622   triggering. Journal of Hydrology, 567, 420-434, 2018.

623   Richards, L.A. Capillary condition of liquids in porous mediums. Physics 1, 318–333, 1931.

624   Schoener, G., Stone, M.C.: Monitoring soil moisture at the catchment scale-A novel approach

625   combing antecedent precipitation index and rader-derived rainfall data, Journal of Hydrology,

626   589, 125155, 2020.

627   Segoni, S., Piciullo, L., Gariano, S.L.: A review of the recent literature on rainfall thresholds for

628   landslide occurrence, Landslides, 15:1483-1501, 2018b.

629   Segoni, S., Rosi, A., Lagomarsino, D., Fanti, R., Casagli, N.: Brief communication: Using averaged

630   soil moisture estimates to improve the performances of a regionalscale landslide early warning

631   system. Nat. Hazards Earth Syst. Sci. 18, 807–812, 2018a.

632   Senthilkumar, V., Chandrasekaran, S.S., Maji, V.B.: Geotechnical characterization and analysis of

633   rainfall-induced 2009 landslide at Marappalam area of Nilgiris district, Tamil Nadu state, India.

634   Landslides, 14, 1803-1814, 2017.

635   Tang, H., Mcguire, L.A., Kean, J.W., Smith, J.B.: The impact of sediment supply on the initiation

636   and magnitude of runoff-generated debris flows. Geophysical Research Letters, 47,

637   e2020GL087643, 2020.

638   Thomas, M.A., Collins, B.D., Mirus, B.B.: Assessing the feasibility of satellite-based thresholds for

639   hydrologically driven landsliding. Water Resource Research, 55, 9006-9023, 2019.

640   Tisdall, A.: Antecedent soil moisture and its relation to infiltration. Aust. J. Agric. Res., 2 (3), 342–

641   348, 1951.

642   Van Genuchten, M.: A closed form equation for predicting the hydraulic conductivity of unsaturated

643   soils. Soil Sci. Soc. Am. J. 44, 892–898, 1980.

644   Wei, F.Q., Hu, K.H., Zhang, J., Jiang, Y.H., Chen, J.: Determination of effective antecedent rainfall

645   for debris flow forecast based on soil moisture content observation in Jiangjia Gully, China. In:

646   DeWrachien, D., Brebbia, C.A., Lenzi, M.A., eds., Monitoring, Simulation, Prevention and

647   Remediation of dense debris flows II. WIT Transactions on Engineering Sciences, England. 13-

648   22, 2008.

649   Yan, Z.Z., Hong, Z.M.: Using the Monte Carlo method to solve integral equations using a modified

650   control variate. Applied mathematics and computation, 242,764-777, 2014.

651   Yang, H.J., Zhang, S.J., Hu, K.H., Wei, F.Q., Wang, K., Liu S.: Field observation of debris flow

652   activities in the initiation area of Jiangjia Gully, Yunnan Province, China, Journal of Mountain

653   Science, 19(6): 1602-1617, 2022.

654   Zeng, Q.L., Yue, Z.Q., Yang, Z.F., Zhang, X.J.: A case study of long-term field performance of

655   check-dams in mitigation of soil erosion in Jiangjia stream, China. Environ Geol 58:897–911,

656   2009.

657   Zhang, S.J., Xu, C.X., Wei, F.Q., Hu, K.H., Xu, H., Zhao, L.Q., Zhang, G.P.: A physics-based model

658   to derive rainfall intensity-duration threshold for debris flow. Geomorphology, 351, 106930, 2020.

659   Zhang, S.J., Yang, H.J., Wei, F.Q., Jiang, Y.H., Liu, D.L.: A model of debris flow forecast based on

660   the water-soil coupling mechanism. Journal of Mountain Science, 25, 757-763, 2014.

661   Zhang, S.J., Xia, M.Y., Li, L., Yang, H.J., Liu, D.L., Wei, F.Q.: Quantify the effect of antecedent

662   effective precipitation on rainfall intensity-duration threshold of debris flow. Landslides, 20,

663   1719-1730, 2023.

664   Zhao, B.R., Dai, Q., Han, D.W., Dai, H.C., Mao, J.Q., Zhuo, L.: Probabilistic thresholds for

665   landslides warning by integrating soil moisture conditions with rainfall thresholds. Journal of

666   Hydrology, 574, 276-287, 2019a.

667   Zhao, B.R., Dai, Q., Han, D., Dai, H., Mao, J., Zhuo, L., Rong, G.: Estimation of soil moisture using

668   modified antecedent precipitation index with application in landslide predictions. Landslides 16,

669   2381–2393, 2019b.

670   Zhu, Y.J., Shao, M.G.: Variability and pattern of surface moisture on a small-scale hillslope in

671   Liudaogou catchment on the northern Loess Plateau of China, Geoderma, 147, 185-191, 2008.

672   Zhuang, J.Q., Cui, P., Wang, G.H., Chen, X.Q., Iqbal, J., Guo, X.J.: Rainfall thresholds for the

673   occurrence of debris flows in Jiangjia Gully, Yunnan Province, China. Eng. Geol. 195, 335–346,

674   2015.